Fast Stochastic MPC with Optimal Risk Allocation Applied to Building Control Systems

Yudong Ma, Sergey Vichik, and Francesco Borrelli

***Abstract*— This paper presents a method for solving linear stochastic model predictive control (SMPC) subject to joint chance constraints. The chance constraints are decoupled using Boole's inequality and by introducing a set of unknowns representing allowable violation for each constraint (the risk). A tailored interior point method is proposed to explore the special structure of the resulting SMPC problem.**

The proposed method is compared with existing two-stage algorithms with the first stage allocating the risks and the second stage optimizing the feedback control gain. The approach is applied to building control problems that minimizes energy usage while keeping thermal comfort by making use of uncertain predictions of thermal loads and ambient temperature. Extensive numerical tests show the effectiveness of the proposed approach.

I. Introduction

The building sector consumes about 40% of the energy used in the United States and is responsible for nearly 40% of greenhouse gas emissions. It is therefore economically, socially, and environmentally significant to reduce the energy consumption of buildings.

Previous work of authors in [1], [2] has focused on developing control oriented models for energy conversion, storage, and distribution in buildings. The models were used in a model predictive control (MPC) scheme with the objective of minimizing energy consumption while satisfying thermal comfort using predictions of weather and occupancy. In the aforementioned works, the MPC scheme uses a nominal deterministic profile of weather and occupancy load. However, in the resulting closed loop control schemes, energy savings and comfort depend on the load predictions which are different from actual realizations. SMPC is a better approach to address this issue when probability distributions of load are available. In this case, we would minimize expected costs and satisfy constraints with a given probability. A thorough review of existing SMPC schemes is reported in [3], [4] and references therein. The integration of SMPC and weather predictions has been investigated by authors in [5]. In [5], the joint chance constraints are approximated assuming that the risk bounds are evenly distributed. In order to reduce the conservatism, the authors in [6] proposed an iterative two-stage optimization procedure to optimize the optimal feedback gain and risk allocations online. The first stage optimizes the linear feedback gain, and the second stage adjusts the risk bounds using iterative risk allocation methods [7], [8].

* Y. Ma, S. Vichik, and F. Borrelli are with the Department of Mechanical Engineering, University of California, Berkeley, CA 94720-1740, USA. E-mail: {myd07, sergv, fborrelli}@berkeley.edu.

In this work, we propose a SMPC problem which seeks the optimal feedback gain and risk allocations simultaneously. The problem is formulated using Boole's inequality to decouple the joint chance constraints, and introducing a set of unknowns to represent allowable violation for each constraint. The resulting non-convex problem then is solved by tailored interior point methods to explore the sparsity of the problem. Simulation results indicate that the proposed method outperforms existing iterative two-stage SMPC in terms of costs and solver time. Additionally, the closed loop performance of the one-stage SMPC provides more energy savings compared to SMPC with fixed risk bounds in [5].

The paper is organized as follow. Section II presents the HVAC system considered in this paper, Section III outlines the SMPC control problem, and a fast tailored interior point method is proposed in Section IV. Simulation results on building HVAC systems and comparison with other approaches are presented in Section V and Section VI.

II. System Description

The main equipments used to produce and distribute cool air in a building are air handling units (AHUs) and variable air volume (VAV) boxes as depicted in Figure 1. The AHU recirculates return air from building spaces, and mixes it with fresh outside air. The proportion of return air to outside air is controlled by damper positions in the AHU (Figure 1). The mixed air is cooled by the cooling coils that extract the cooling energy from chilled water produced by chillers.

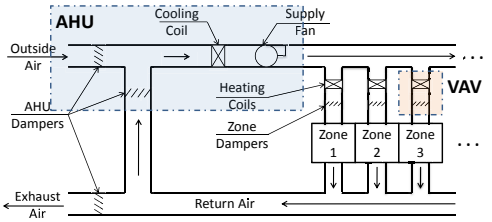

Fig. 1: Schematics of the air distribution system.

The air temperature after the cooling coil depends on the cooling coil valve position, the temperature of the chilled water, the temperature of mixed air entering the cooling coil, the mass flow rate of the mixed air, and the physical characteristics as well as thermal effectiveness of the cooling coil. Cool air is delivered to the building spaces by electrical fans. Before reaching a given space, the air goes through variable air volume (VAV) boxes. At each VAV box the

mass flow rate of the air supplied to the space is adjusted by the position of a damper. In addition, air temperature can be increased using reheat coils installed in the VAV box when needed. The space served by one VAV box is denoted by a thermal zone. The delivered air enters a zone through diffusers that are designed to fully mix the incoming air with the air in thermal zone.

The temperature dynamics of a network of zones can be modeled as a RC network [9] and a set of nonlinear regression models in [10]. Both models can be compactly written as:

$$x_{k+1} = f_z(x_k, u_k, w_k), \tag{1a}$$
$$T_k = g_z(x_k, w_k), \tag{1b}$$

where x_k is the state of the system at time k, T_k is the vector collecting the perceived temperature of each zone, u_k is the control inputs from AHU and VAV boxes, and w_k is the disturbances including the ambient temperature and disturbance load for each zone. In this paper, the disturbance w_k is stochastic in nature, and the statistics of w_k are calculated using historical data. We present the fast stochastic MPC design with optimal risk allocation in the following sections. The detailed zone models are introduced later with the simulation results.

III. Problem Formulation

Non-linearities in the dynamic equations of a stochastic MPC problem lead to an intractable problem with increasing number of zones. The approach that we use in this paper is to solve the nonlinear stochastic MPC problem by computing the solution to a series of time-varying linear stochastic MPC subproblems. The time varying linear system is obtained by iteratively linearizing the nonlinear system around the current solution. This procedure repeats until a convergence condition is met. To keep formulations simple, we focus on fast stochastic MPC design for time varying linear systems in the remainder of the paper.

Consider the following time varying linear stochastic MPC problem with joint chance constraints:

$$\min_{x,u} J = \sum_{k=0}^{N-1} \mathbb{E}\{x_k^T Q_k x_k + {c_k^x}^T x_k + u_k^T R_k^u u_k + {c_k^u}^T u_k\} + \mathbb{E}\{x_N^T Q_N x_N\} \tag{2a}$$

subj. to:

$$x_{k+1} = A_k x_k + B_k u_k + D_k w_k, \quad k = 0, 1, \ldots, N-1, \tag{2b}$$

$$\Pr\{\bigcup_{k=1}^{N} x_k \notin \mathcal{F}_k^x\} \le \alpha_x, \ \Pr\{\bigcup_{k=0}^{N-1} u_k \notin \mathcal{F}_k^u\} \le \alpha_u, \tag{2c}$$

where α_x (α_u) is the total allowable probability violation of state (input) constraints, $x_k \in \mathbb{R}^{n\times 1}$ is the system state at time instance k, $u_k \in \mathbb{R}^{m\times 1}$ collects the control inputs, and w_k is the process disturbance assumed to be Gaussian random variable, i.e. $w_k \sim \mathcal{N}(\hat{w}_k, \Sigma_k)$. $\mathcal{F}_k^x$ and $\mathcal{F}_k^u$ are the feasible sets of the system states x_k and control inputs u_k, respectively. Q, R^u, c^x, and c^u are the penalty matrices. The feasible regions are assumed to be polyhedra:

$$\mathcal{F}_k^x = \left\{x_k | {h_{ki}^x}^T x_k \le g_{ki}^x, i = 1, 2, \ldots, M_x.\right\}, \tag{3a}$$
$$\mathcal{F}_k^u = \left\{u_k | {h_{ki}^u}^T u_k \le g_{ki}^u, i = 1, 2, \ldots, M_u.\right\}. \tag{3b}$$

Three steps are necessary to solve the SMPC problem (2): 1) the propagation of the statistics of system states and inputs (2b), 2) the evaluation of the joint chance constraint (2c), and 3) the solution the resulting nonlinear program (2).

Details of these steps are presented in following sections.

A. System Propagation

It is assumed that a linear feedback control law

$$u_k = \hat{u}_k + K_k(x_k - \hat{x}_k) \tag{4}$$

is applied to system (2b). The mean of the control input is $\hat{u}_k$, and the feedback gain K_k is time varying. Because of the Gaussian distribution of the disturbance w_k and the linearity of the system (2b), the system state x_k is a Gaussian random variable with mean $\hat{x}_k$ and variance Ω_k, i.e. $x_k \sim \mathcal{N}(\hat{x}_k, \Omega_k)$. The mean $\hat{x}_k$ and variance Ω_k of the resulting closed loop system states are computed as

$$\hat{x}_{k+1} = A_k \hat{x}_k + B_k \hat{u}_k + D_k \hat{w}_k \tag{5a}$$
$$\Omega_{k+1} = (A_k + B_k K_k)\Omega_k (A_k + B_k K_k)^T + D_k \Sigma_k D_k^T, \tag{5b}$$
$$\hat{x}_0 = \hat{x}(0), \ \Omega_0 = \Omega(0), \tag{5c}$$

where $\hat{x}(0)$ ($\Omega(0)$) is the measured or estimated mean (variance) of the current state. The variance matrix Π_k of the control inputs is computed as $\Pi_k = K_k \Omega_k K_k^T$.

B. Chance Constraints

Direct integration of the multivariate Gaussian density function (2c) is computationally intensive [11]. In this work, we use the classical approach of decoupling the joint chance constraints (2c) into individual chance constraints using Boole's inequality [12]. The probability that at least one of the violations happens is no greater than the sum of the probabilities of individual violation.

$$\Pr\{\bigcup_{k=1}^{N} x_k \notin \mathcal{F}_k^x\} \le \sum_i \sum_k \Pr\{{h_{ki}^x}^T x_k > g_{ki}^x\} \le \alpha_x, \tag{6a}$$
$$\Pr\{\bigcup_{k=1}^{N} x_k \notin \mathcal{F}_k^x\} \le \sum_i \sum_k \Pr\{{h_{ki}^x}^T x_k > g_{ki}^x\} \le \alpha_x, \tag{6b}$$

Then, the joint chance constraints (2c) then can be conservatively approximated as

$${h_{ki}^x}^T \hat{x}_k - g_{ki}^x + \beta_{ki}^x \sqrt{{h_{ki}^x}^T \Omega_k h_{ki}^x} \le 0, \tag{7a}$$
$${h_{ki}^u}^T \hat{u}_k - g_{ki}^u + \beta_{ki}^u \sqrt{{h_{ki}^u}^T \Pi_k h_{ki}^u} \le 0, \tag{7b}$$
$$\sum_{k=1}^{N} \sum_{i=1}^{M_x} 1 - \text{cdf}(\beta_{ki}^x) \le \alpha_x, \ \sum_{k=0}^{N-1} \sum_{i=1}^{M_u} 1 - \text{cdf}(\beta_{ki}^u) \le \alpha_u, \tag{7c}$$

where $\beta_{ki}^x \ge 0$ ($\beta_{ki}^u \ge 0$) is the risk bound reflecting the allowable violation for each individual state (input) chance constraint α_{ki}^x (α_{ki}^u), $\alpha_{ki}^x = 1 - \text{cdf}(\beta_{ki}^x)$, $\alpha_{ki}^u = 1 - \text{cdf}(\beta_{ki}^u)$, and $\text{cdf}(\cdot)$ is the cumulative density function defined as $\text{cdf}(\beta) = \frac{1}{\sqrt{2\pi}} \int_{-\infty}^{\beta} \exp^{-\frac{z^2}{2}} dz$. Note that a solution to (7) is also a feasible solution to the joint chance constraints (2c).

C. Optimization Problem

The stochastic MPC problem with joint chance constraints (2) now can be explicitly formulated as the deterministic optimization problem by replacing chance constraints (2c) by (7), and by substituting dynamic system (2b) by (5).

In this article we show how to compute the solution to the SMPC problem by exploring the sparse structure of the problem and properly choosing the initial guess for problem (2). Note that the SMPC problem (2) optimizes both the feedback gain and risk allocations simultaneously.

In order to show the sparse structure of the problem, the optimization problem (2) is rewritten compactly as,

$$\min_{z} \; J(z) \tag{8a}$$

$$\text{subj. to:} f(z) = 0, \tag{8b}$$

$$h_c(z) <= 0, \tag{8c}$$

$$h_\beta(z) <= 0, \tag{8d}$$

where $z = [\hat{u}_0; \text{vec}(K_0); \beta_0^u; \hat{x}_1; \text{vec}(\Omega_1); \beta_1^x; \hat{u}_1; \text{vec}(K_1); \beta_1^u; \ldots; \hat{x}_N; \text{vec}(\Omega_N); \beta_N^x]$ collects the optimization variables. $\text{vec}(X)$ is the operation to stack the columns of X into a single column vector.

According to [13], it is simple to show that the Jacobian matrix of $f(z)$ has a banded structure, the Jacobian matrix of $h_c(z)$ has a block diagonal structure, and the Jacobian matrix of $h_\beta(z)$ is a full matrix.

Let ρ, λ_c, and λ_β be the dual variables for constraints (8b), (8c), and (8d), respectively. Then the Lagrangian function of problem (8) is defined as

$$L(z, \rho, \lambda) = J(z) + \rho^T f(z) + \lambda_c^T h_c(z) + \lambda_\beta^T h_\beta(z).$$

The Hessian matrix of the lagrangian function is block diagonal. In the following sections, we present a primal-dual interior point method to exploit the sparsity of the Jacobian and Hessian matrices so that problem (8) is solved efficiently.

IV. Fast Primal-Dual Interior Point Method

Problem (8) is reformulated by adding slack variables, and replacing the nonnegativity constraints with a logarithmic barrier term in the objective function,

$$\min_{z,s,t,y} \; J(z) - \mu \left(\sum_i \log(s_i) + \sum_i \log(t_{ci}) + \sum_i \log(t_{\beta i}) + \sum_i \log(y_i) \right), \tag{9a}$$

$$\text{subj. to:}$$

$$f(z) + s = 0, \tag{9b}$$

$$h_c(z) + t_c = 0, \quad h_\beta(z) + t_\beta = 0, \tag{9c}$$

$$s + y = 0. \tag{9d}$$

The computation of the solution to (8) involves the following steps [14]:

- S0 find an initial feasible guess z^0 or with associated minimal constraint violation in 1-norm,
- S1 calculate a descent direction by solving the KKT system of problem (9),
- S2 update the penalty weight μ so that the solutions to (9) approaches the one of (8),
- S3 select a step length to update the primal and dual variables of problem (9),
- S4 iterate procedures S1 to S4 until the algorithm converges to a (local) optimum.

With the exception of S1, the steps S0–S4 are standard in the literature [14]. In S1, a tailored Cholesky decomposition is developed to explore the sparse structure of problem (9). The details of S0 and S1 are discussed in the following sections, and standard procedures for S2-S4 are reported in [13].

A. Initial Guess

The initial guess is chosen as follow.

1) The risk bounds for each state and input chance constraint are evenly assigned,

$$\beta_{ki}^{u\,0} = \text{cdf}^{-1}(\frac{\alpha_u}{NM_u}), \; \beta_{ki}^{x\,0} = \text{cdf}^{-1}(\frac{\alpha_x}{NM_x}). \tag{10}$$

2) The linear feedback gain K_k^0 is initialized by solving the unconstrained LQR problem. For fixed feedback gain K_k^0 in control policy (4), the variance of the states Ω_k^0 can be propagated by equation (5b).

3) With fixed K_k^0, $\beta_{ki}^{u\,0}$, Ω_k^0, and $\beta_{ki}^{x\,0}$, the optimization problem (2) is reduced to a linear programming, and efficient and robust solvers are available to obtain x_k^0 and u_k^0. If the reduced linear programming is infeasible, the chance constraints (2c) are relaxed as soft constraints, and the constraint violations are penalized using 1-norm. Let z^0 be the initial guess to Problem (8).

4) The slack variables s, t, and y in problem (9) are initialized as

$$s^0 = \max(-f(z^0), 10), \quad t_c^0 = \max(-h_c(z^0), 10),$$
$$t_\beta^0 = \max(-h_\beta(z^0), 10), \quad y^0 = \max(-s^0, 10).$$

B. Descent Direction

Given an initial guess to Problem (9), the descent direction to update the candidate solution to Problem (9) is computed by solving the linearized KKT conditions.

As reported in [13], linearized KKT conditions can be reduced to the following linear systems,

$$\Psi \Delta z = -\tilde{r}_z^j - [\nabla f^T, \; \nabla h_\beta^T] \begin{bmatrix} \Delta\rho \\ \Delta\lambda \end{bmatrix}, \tag{12a}$$

$$Z \begin{bmatrix} \Delta\rho \\ \Delta\lambda \end{bmatrix} = \begin{bmatrix} \tilde{r}_\rho^j \\ \tilde{r}_\lambda^j \end{bmatrix} - \begin{bmatrix} \nabla f \\ \nabla h \end{bmatrix} \Psi^{-1} \tilde{r}_z^j, \tag{12b}$$

where Δz ($\Delta\rho$ and $\Delta\lambda$) are the descent direction for primal (dual) variables, and derivations of the coefficients ($\tilde{r}_\rho$, $\tilde{r}_\lambda$, $\tilde{r}_z$, Z, and Ψ) are reported in [13]. Ψ is a block diagonal matrix, and Z is arrowhead matrix due to the sparse structure of Ψ, ∇f, and ∇h_β.

$$Z = \begin{bmatrix} Z_1^1 & Z_1^2 & 0 & \cdots & 0 & 0 & Z_{N+1}^{1\,T} \\ Z_2^1 & Z_2^2 & Z_2^3 & \cdots & 0 & 0 & Z_{N+1}^{2\,T} \\ 0 & Z_3^2 & Z_2^2 & \cdots & 0 & 0 & Z_{N+1}^{3\,T} \\ \vdots & \vdots & \vdots & \ddots & \vdots & \vdots & \\ 0 & 0 & 0 & \cdots & Z_{N-1}^{N-1} & Z_{N-1}^{N} & Z_{N+1}^{N-1\,T} \\ 0 & 0 & 0 & \cdots & Z_N^{N-1} & Z_N^N & Z_{N+1}^{N\,T} \\ Z_{N+1}^1 & Z_{N+1}^2 & Z_{N+1}^3 & \cdots & Z_{N+1}^{N-1} & Z_{N+1}^N & Z_{N+1}^{N+1} \end{bmatrix}.$$

The system (12b) is solved by Cholesky factorization of matrix Z followed by forward and backward substitution. The Cholesky factorization of Z is carried out as $Z = LL^T$, where L is a lower triangular matrix

$$L = \begin{bmatrix} L_1^1 & 0 & 0 & \cdots & 0 & 0 & 0 \\ L_2^1 & L_2^2 & 0 & \cdots & 0 & 0 & 0 \\ 0 & L_3^2 & L_2^2 & \cdots & 0 & 0 & 0 \\ \vdots & \vdots & \vdots & \ddots & \vdots & \vdots & \vdots \\ 0 & 0 & 0 & \cdots & L_{N-1}^{N-1} & 0 & 0 \\ 0 & 0 & 0 & \cdots & L_N^{N-1} & L_N^N & 0 \\ L_{N+1}^1 & L_{N+1}^2 & L_{N+1}^3 & \cdots & L_{N+1}^{N-1} & L_{N+1}^N & L_{N+1}^{N+1} \end{bmatrix},$$

where L_{ii} is lower triangular. By expressing out $Z = LL^T$, we have

$$L_1^1 L_1^{1T} = Z_1^1, \tag{13a}$$
$$L_i^i L_{i+1}^{i\ T} = Z_i^{i+1},\ i = 1, 2, \ldots, N-1, \tag{13b}$$
$$L_i^i L_i^{iT} = Z_i^i - L_i^{i-1} L_i^{i-1T},\ i = 2, 3, \ldots, N, \tag{13c}$$
$$L_1^1 L_{N+1}^{1\ T} = Z_{N+1}^{1\ T}, \tag{13d}$$
$$L_i^i L_{N+1}^{i\ T} = Z_{N+1}^{i\ T} - L_i^{i-1} L_{N+1}^{i-1\ T},\ i = 2, 3, \ldots, N, \tag{13e}$$
$$L_{N+1}^{N+1} L_{N+1}^{N+1T} = Z_{N+1}^{N+1} - \sum_{i=1}^{N} L_{N+1}^i L_{N+1}^{i\ T}. \tag{13f}$$

Thus each block in L can be computed by Cholesky factorization and forward substitution.

The Cholesky factorization of Z provides an efficient and robust method to calculate $\Delta\rho$ and $\Delta\lambda$, and Δz can be obtained by solving equation (12a). after the evaluation of Z.

V. Simulation Result A

This section presents numerical results to show the effectiveness of the proposed approach. In this example, two interconnected zones are considered, and the control objective is to maintain zone temperatures within comfort range. A quadratic function of the control inputs is minimized.

The dynamic zone model is formulated as follows,

$$C_1 \frac{dT_1}{dt} = u_1^h - u^c + \frac{T_{oa} - T_1}{R_1^a} + \frac{T_2 - T_1}{R} + P_1, \tag{14a}$$
$$C_1 \frac{dT_2}{dt} = u_2^h - u^c + \frac{T_{oa} - T_2}{R_2^a} + \frac{T_1 - T_2}{R} + P_2, \tag{14b}$$

where C_k captures the lumped up thermal capacitance of k-th zone, R_k^a represents the thermal resistance of zone walls isolating zone air from ambient environment of temperature T_{oa}, and R is the thermal resistance of the walls separating Zone 1 and Zone 2. The perceived air temperatures of Zone 1 and Zone 2 are represented by T_1 and T_2, respectively. P_k is the disturbance load of zone k induced by solar radiation, occupancy, and electrical devices. The zone temperatures are regulated by the centralized cooling energy input $u^c \geq 0$, and distributed heating energy input $u_k^h \geq 0$ for each zone.

The model (14) is discretized using trapezoidal method with a sampling time of Δt, and the resulting discrete time model is compactly rearranged,

$$T_{k+1} = AT_k + Bu_k + Dw_k, \tag{15}$$

where $T = [T_1; T_2]$ collects the zone temperatures, $u = [u_1^h;\ u_2^h;\ u^c]$ is the heating and cooling energy inputs, and $w = [P_1; P_2; T_{oa}]$ is the system disturbances.

The comfort constraints of zones are defined as follows. The perceived zone temperature T is constrained between 18 ^{o}C and 28 ^{o}C before 6:00 when the zones are vacant, and after 7:00 the comfort set is shrunk to [21, 25]^{o}C when the zones are loaded with occupants till 20:00. The control input $u \geq 0$ is upper bounded by 8kW due to power limits of the heating and cooling devices.

The parameters used in this example are listed in Table I.

TABLE I: Parameters

parameter	value	parameter	value
C_1	1.10e4 J/^{o}C	C_2	1.28e4 J/^{o}C
R_1	41.67 ^{o}C/W	R_2	35.71 ^{o}C/W
R	35.00 ^{o}C/W	Δt	1 hour
Q	0	c^x	0
R^u	eye(3)	c^u	0
N	12	ϵ	1e-4
α_x	0.15	α_u	0.05

The weather information is downloaded from July 2nd to July 3rd, 2009 at UC Berkeley, and it is assumed that the uncertainty of the weather predictions is Gaussian distributed with one standard deviation of $\sigma_{Toa} = 0.71^o$C. The disturbance loads P_1 and P_2 are assumed to include a constant loads of 0.1kW due to workstations and servers running 24 hours a day, and an occupancy load of 10 kW between 7:00 to 17:00 everyday. The uncertainty of the disturbance loads are assumed to be normal distributed with a standard deviation of $\sigma_P = 0.63$kW.

The fast stochastic MPC algorithm (FIP) is compared with existing two-stage optimization methods proposed in [6], [7]. The following algorithms are tested.

- FIP Fast interior point method proposed in Section IV.
- IBS Two-stage optimization method presented by authors in [6]. The first stage iteratively adjusts the risk bounds using bisection method, and the second stage optimizes the feedback gain with fixed risk allocation.
- IRA Two-stage optimization method proposed in [7]. The first stage optimizes the feedback gain with fixed risk allocation. The second stage then increases the allowable violations of active constraints while bounding the total allowable constraint violations.
- IOA Two-stage optimization method proposed in [8]. The first stage optimizes the risk bounds with fixed linear feedback gain by solving a convex optimization problem [8], and the second stage optimizes the feedback gain with fixed risk allocation.

The algorithms above are coded in Matlab® and run on a PC with Intel Dual Core CPU 3.00GHz. The optimization problems of the lower stage of IBS, IRA, and IOA algorithms are formulated as second order cone problems using disturbance feedback [15], and the resulting problems are solved by IBM ILOG CPLEX Optimization Studio®.

Figure 2 shows the costs and solver time of the four algorithms when the zone temperatures are initialized with twenty different realizations evenly selected from 21^{o}C to 26 ^{o}C. Both the cost and solver time are normalized over the results of FIP algorithm. The results indicate that the proposed algorithm converges to a lower cost in less time.

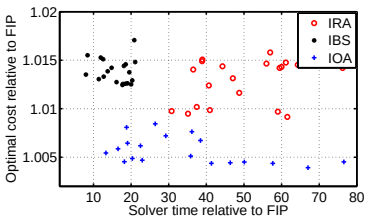

Fig. 2: Algorithms' comparison

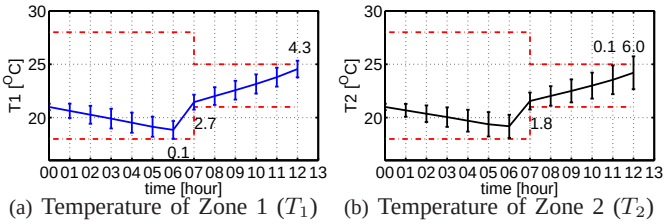

(a) Temperature of Zone 1 (T_1) (b) Temperature of Zone 2 (T_2)

Fig. 3: Zone temperatures

Figure 3 plots the zone temperatures T_1 and T_2 within three standard deviations from the mean when FIP is used to solve the temperature regulation problem. The dashed lines are the comfort constraints. The results shows that the proposed SMPC method only allocates allowable violations to some constraints, and they are indicated by the numbers in Figure 3. For example, in Figure 3(b), the temperature of Zone 2 is allowed to violate the lower comfort constraints at 7:00 with a chance of 1.8%, and 6.0% of possible realizations of T_2 is permitted to violate the upper comfort constraints at 12:00. It is noted that the allowable comfort constraint violations for both T_1 and T_2 sum up to $\alpha_x = 15\%$.

VI. Simulation Result B

In this example, the one-stage stochastic MPC with optimal risk allocation (FIP) is applied to the HVAC system serving the second floor of DOE library at UC Berkeley. The second floor of DOE library consists of 16 thermal zones. In this example, we present the results for zone 5 and zone 15. Each zone is controlled by a VAV box that consists of a heating coil and a damper. The heating coil controls the supply air temperature to each zone T_s by heating up the supply air from air handler units with temperature of T_{AHU} when necessary, and the damper position regulates the supply air mass flow rate to each zone $\dot{m}$.

The identified zone model is a third order, auto regressive bilinear model as follow,

$$\begin{aligned} T_i^{k+1} = {} & b_{1,i}T_{oa}^k + b_{2,i}T_{oa}^{k-1} + b_{3,i}T_{oa}^{k-2} + b_{4,i}(T_{s,i}^k - T_i^k)\dot{m}^k \\ & + b_{5,i}I_i^k + b_{6,i}I_i^{k-1} + b_{7,i}I_i^{k-2} + b_{8,i} \\ & + b_{9,i}T_i^k + b_{10,i}T_i^{k-1} + b_{11,i}T_i^{k-2} + P_i^k, \end{aligned} \tag{16}$$

where $i \in \{5, 15\}$ is the zone index, $b_{j,i}$ are the model coefficients for zone i, T_{oa}^k is the ambient temperature at time k, $T_{s,i}^k$ is the supply air temperature to zone i, $\dot{m}_i^k$ is the supply mass flow rate to zone i, I_i^k is the sun load intensity for zone i and T_i^k is the zone i temperature at time k, and P_i^k is the temperature increased due to the disturbance load induced by occupants in zone i.

The uncertainty model for disturbances including occupancy load, sun load, and ambient temperature, and the uncertainties are modeled using data collected from December 1st, 2011 to January 31st, 2012 at the DOE library at UC Berkeley. More details of the zone model and the uncertainty models are reported in [16].

The disturbance load induced by solar radiation for each zone is computed as the measured sun radiation intensity projected onto the norm vector to the outside wall. The sun radiation intensity is downloaded from the nearest weather station. Figure 4 lumps up the computed daily sun load for zone 5 from December 1st, 2011 to January 31st, 2012 in DOE library at UC Berkeley. The mean and variance of the sun load are evaluated using historical measurements.

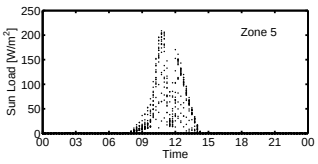

Fig. 4: Solar load

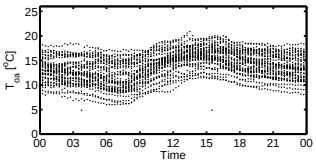

Fig. 5: Ambient temperature.

The historical ambient temperature from December 1st, 2011 to January 31st, 2012 plotted in Figure 5 is obtained from the local weather station. The ambient temperature uncertainty is assumed normal distributed, and the statistics can be computed from the historical observations in Figure 5.

The occupancy loads are calculated as the difference between the historical temperature measurements and the predicted zone temperatures by model (16). Figure 6 lumps up the computed daily occupancy loads from December 1st, 2011 to January 31st, 2012 in DOE library at UC Berkeley.

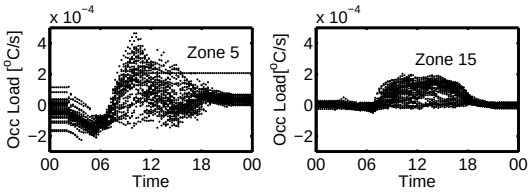

Fig. 6: Occupancy load

The components that use energy include dampers, supply fans, and heating coils. The supply fan needs electrical power to drive the system, the heating coils consume the energy of hot water, and the power to drive the dampers is assumed to be negligible. A simple energy consumption model for each component has been presented in [9], and the simplified energy models are listed here for the sake of completeness.

The fan power can be approximated as a second order polynomial function of the total supply air mass flow rate ($\dot{m} = \sum_{i\in\{5,15\}} \dot{m}_i$) driven by the fan.

$$E_f = c_0 + c_1\dot{m} + c_2\dot{m}^2, \tag{17}$$

where c_0, c_1, c_2 are parameters to be identified.

Heating coils are air-water heat exchangers, and the power consumption of the heating coils are

$$E_{h\,i} = \frac{c_p\dot{m}_{s\,i}(T_{s\,i} - T_{AHU})}{\eta_h\,\mathrm{COP}_h}, \tag{18}$$

where $E_{h\,i}$ is the power used to generate the hot water consumed by the heating coils in the VAV box connected with room i, η_h is the conversion efficiency of the hating coil, and COP_h is the heating coefficient of performance.

The total electricity power consumption of the HVAC system over the prediction horizon then is calculated as $E_{\text{tot}} = \sum_{k=0}^{k=N} (\sum_{i\in\{5,15\}} E_{h\,i}^k + E_f^k)\Delta t$.

In this numerical example, the control sampling time is $\Delta t = 15$ min, and the prediction horizon is $N = 4$. The comfort set is described in Section V, and the control input constraints are defined as follow

$$\dot{m}_{s\,i} \in [0, 35]\text{kg/s},\ T_{s\,i} \in [T_{AHU}, 42]^o\text{C}, i \in \{5, 15\}.$$

The total allowable state (input) constraint violation is $\alpha_x = 20\%$ ($\alpha_u = 10\%$).

The closed loop performance of FIP is compared with the SMPC approach with fixed evenly distributed risk bounds (SMPC-F) [5], i.e. each individual state (input) constraint is allowed to violate with a chance of $\frac{\alpha_x}{NM_x}$ ($\frac{\alpha_u}{NM_u}$).

The controllers FIP and SMPC-F are simulated in closed loop with model (16) for one day. The realizations of disturbances are assumed to be the mean values.

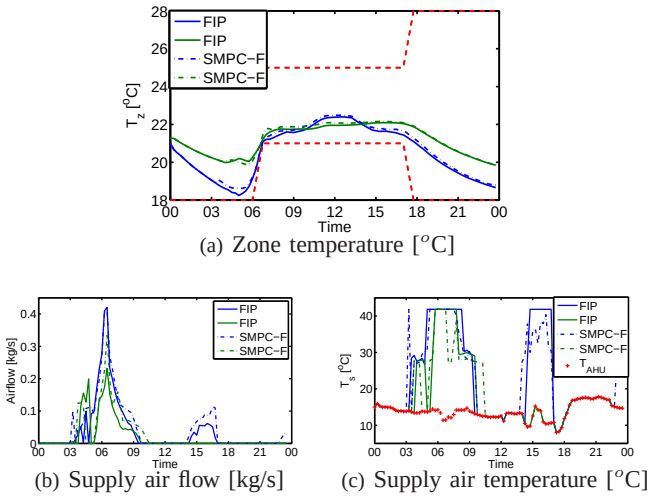

(a) Zone temperature [^{o}C]

(b) Supply air flow [kg/s]

(c) Supply air temperature [^{o}C]

Fig. 7: Simulation results

Simulation results are reported in Figure 7. In Figure 7(a), the dashed lines are comfort constraints, and the solid (dash-dot) lines represent the zone temperatures when FIP (SMPC-F) is implemented. Compared to SMPC-F with fixed risk allocation, FIP controls the zone temperatures closer to lower bounds due to its capability to adjust the risk over the prediction horizon. Figures 7(b) and 7(c) plot the supply air mass flow rate $\dot{m}$ and the supply air temperature T_s from VAV boxes, respectively. The line marked by cross in Figure 7(c) depicts the supply air temperature from AHU T_{AHU}. The HVAC system controlled by FIP consumes 13.7% less total energy than SMPC-F with fixed risk allocation. The closed loop simulation is also performed for less allowable constraint violations $\alpha_x = 10\%$, $\alpha_u = 5\%$, and the total energy savings of FIP over SMPC-F is reduced to 6.8%. FIP requires less energy to maintain zone temperatures within the thermal comfort for a specific probability level. The introduction of risk allocation reduces the conservativeness of SMPC scheme.

Acknowledgment

This material is based upon work supported by the National Science Foundation under Grant No. 0844456. Any opinions, findings, and conclusions or recommendations expressed in this material are those of the authors and do not necessarily reflect the views of the National Science Foundation.

References

[1] Y. Ma, F. Borrelli, B. Hencey, B. Coffey, S. Bengea, and P. Haves, "Model predictive control for the operation of building cooling systems," *Control Systems Technology, IEEE Transactions on*, vol. 20, pp. 796–803, May 2011.

[2] Y. Ma and F. Borrelli, "A distributed predictive control approach to building temperature regulation," in *2011 American Control Conference*, June 2011.

[3] D. Van Hessem, C. Scherer, and O. Bosgra, "LMI-based closed-loop economic optimization of stochastic process operation under state and input constraints," in *Decision and Control, 2001. Proceedings of the 40th IEEE Conference on*, vol. 5, pp. 4228 –4233 vol.5, 2001.

[4] M. Cannon, B. Kouvaritakis, and X. Wu, "Probabilistic Constrained MPC for Multiplicative and Additive Stochastic Uncertainty," *Automatic Control, IEEE Transactions on*, vol. 54, no. 7, pp. 1626–1632, 2009.

[5] F. Oldewurtel, A. Parisio, C. Jones, M. Morari, D. Gyalistras, M. Gwerder, V. Stauch, B. Lehmann, and K. Wirth, "Energy Efficient Building Climate Control using Stochastic Model Predictive Control and Weather Predictions," in *American Control Conference*, (Baltimore, USA), June 2010.

[6] M. P. Vitus and C. J. Tomlin, "On feedback design and risk allocation in chance constrained control," in *Proceedings of the 50th IEEE Conference on Decision and Control*, (Orlando, Florida), December 2011.

[7] M. Ono and B. Williams, "Iterative risk allocation: A new approach to robust model predictive control with a joint chance constraint," in *Decision and Control, 2008. CDC 2008. 47th IEEE Conference on*, pp. 3427 –3432, December 2008.

[8] L. Blackmore and M. Ono, "Convex chance constrained predictive control without sampling," *Jet Propulsion*, vol. 4800, no. 1, pp. 0–6, 2009.

[9] Y. Ma, A. Kelman, A. Daly, and F. Borrelli, "Predictive control for energy efficient buildings with thermal storage: Modeling, stimulation, and experiments," *Control Systems, IEEE*, vol. 32, pp. 44 –64, February 2012.

[10] J. Jang, *System Design and Dynamic Signature Identification for Intelligent Energy Management in Residential Buildings*. PhD thesis, University of California at Berkeley, 2008.

[11] A. Charnes and W. W. Cooper, "Chance-constrained programming," *Management Science*, vol. 6, no. 1, pp. 73–79, 1959.

[12] L. Blackmore, H. Li, and B. Williams, "A probabilistic approach to optimal robust path planning with obstacles," in *in Proceedings of the American Control Conference*, 2006.

[13] Y. Ma, S. Vichik, and F. Borrelli, "Fast stochastic mpc with optimal risk allocation applied to building control systems," tech. rep., University of California at Berkeley, 2012. `http://www.mpc.berkeley.edu/people/yudong-ma/files/YudongMa_CDC12_ver1.pdf`.

[14] D. F. Shanno and R. J. Vanderbei, "Interior-point methods for non-convex nonlinear programming: Orderings and higher-order methods," tech. rep., MATH. PROG, 1999.

[15] J. Löfberg, "Approximations of closed-loop MPC," in *IEEE Conference on Decision and Control*, (Maui, Hawaii), pp. 1438–1442, December 2003.

[16] S. Vichik and F. Borrelli, "Identification of thermal model of DOE library," tech. rep., University of California at Berkeley, 2012. `http://www.mpc.berkeley.edu/people/sergey-vichik/file/SystemID_DOE_Library.pdf`.